Antibonding plasmon mode coupling of an individual hole in a thin metallic film

J. W. Lee,[1] T. H. Park,[2] Peter Nordlander,[2] and Daniel M. Mittleman[1,*]
[1]*Department of Electrical and Computer Engineering, Rice University, 6100 Main Street, Houston, Texas 77005, USA*
[2]*Department of Physics and Astronomy, Rice University, 6100 Main Street, Houston, Texas 77005, USA*
(Received 5 October 2009; published 18 November 2009)

The polarization dependence of the optical properties of individual subwavelength holes in a thin metallic film is studied using terahertz time-domain spectroscopy. We show that for parallel polarization of the incident light, the coupling is predominantly to short-range bonding film plasmons while for perpendicular polarization the incident light couples more efficiently to long-range antibonding film plasmons. These results represent a direct observation of antisymmetric hybridized plasmons and clarify the nature of plasmonic excitations in metallic structures with subwavelength-scale geometrical features. They show that polarization can be used as a means for selective excitation of film plasmon modes.

DOI: 10.1103/PhysRevB.80.205417 PACS number(s): 78.20.Ci, 73.20.Mf, 78.66.Bz, 87.50.U−

Plasmonics in metallic subwavelength structures has been the inspiration for much research in the study of fundamental light-matter interactions as well as in developments of new photonic technologies.[1,2] In particular, the ability to accumulate and control the electromagnetic field at subwavelength scales is critical for the development of active optical systems such as plasmon-based solar cells,[3] optical antennas,[4–6] and photonic and optoelectronic devices for biological and chemical sensing.[7] Despite intense studies of surface plasmons at metal-dielectric interfaces[8,9] and of the optical properties of metallic surfaces with subwavelength structural defects,[10–15] many fundamental questions remain unanswered. For instance, for parallel polarization, i.e., the in-plane polarization component, of the incident light toward a single circular hole in a thin metallic film, the appearance of resonant behavior has been explained as the excitation of a localized hole plasmon with a dipolar charge oscillation in the plane of the aperture[10] or, alternatively, as the effect of guided modes.[11–15] However, no studies have been performed for light polarized perpendicularly to the surface.

The hole plasmon resonance (HPR) is not only responsible for the induced dipole moment around the hole but is also coupled to the plasmon modes of the extended metal film.[16,17] Using the plasmon hybridization method, it has been shown that the dispersion relations of the plasmon modes of a thin metallic film with a hole are the same as those of a continuous film. In the presence of a hole, among many plasmon modes, the particular bonding film plasmon modes for which half of their spatial wavelength is equal to the hole diameter induce a dipole moment across the hole. Thus the HPR is revealed when the incident light frequency is resonant to a film plasmon mode of half wavelength equal to the hole diameter. This theoretical explanation was experimentally confirmed by showing that the HPR exhibit strong redshift with increasing hole diameter or decreasing film thickness.

In the case of a thin film, the surface-plasmon modes on the two film surfaces interact electromagnetically and give rise to hybridized film plasmon modes. The lower-energy bonding mode has a symmetric alignment of surface charges on the two surfaces of the film and the higher-energy antibonding mode has an antisymmetric charge alignment.[18,19] While the bonding film plasmon mode is strongly damped and commonly referred to as the "short-range" mode, the antibonding mode exhibits less attenuation and propagates over longer distances. This "long-range" film plasmon mode is therefore of considerable interest in plasmonic waveguide applications.[20–22] Due to the momentum mismatch between surface plasmons and photons, film plasmons cannot be excited directly using incident plane waves. To accomplish such excitations, one can use either evanescent excitation,[21] periodic corrugation of the film,[22] or antennas.[23] For the development of metallic films as efficient subwavelength plasmonic waveguides there is clearly a need to develop antennas that can couple light efficiently into long-range film plasmons.

In this paper, we show that an individual hole in the film can serve as an antenna for exciting both short- and long-range film plasmon modes. We perform azimuth-angle-dependent transmission measurements using terahertz time-domain spectroscopy. For parallel polarization, we find that only short-range film plasmons are excited. As the polarization angle becomes more perpendicular a second feature appears in the transmission spectra corresponding to the excitation of long-range film plasmon modes. The energies of the short- and long-range modes are found to depend strongly on the diameter of the hole in excellent agreement with a simple and intuitive model based on plasmon hybridization.[16]

For a metallic film with thickness t in vacuum, the dispersion relations of the film plasmons including retardation effects can be calculated from the Maxwell equations associated with the boundary conditions for the metal-dielectric interfaces

$$\gamma_1\varepsilon_0 + \gamma_0\varepsilon_1 = \pm e^{-\gamma_1 t}(\gamma_1\varepsilon_0 - \gamma_0\varepsilon_1), \tag{1}$$

where $\varepsilon_i(i=0,1)$ is the dielectric function in vacuum and metal, respectively. Here, for metal film $\varepsilon_1(\omega)$, we simply use the Drude model as $\varepsilon_1(\omega)=1-\omega_B^2/\omega^2$ and ω_B is the bulk-plasmon frequency of the metal. The quantities γ_i are the perpendicular components of the wave vector and have the form $\gamma_i^2=k^2-\varepsilon_i(\omega/c)^2$, where k is the magnitude of a planar surface-plasmon wave vector and c is the speed of light in vacuum.

In Fig. 1, we show the calculated plasmon dispersions for films of thickness 0.01, 0.05, and 10 microns. For a thin film

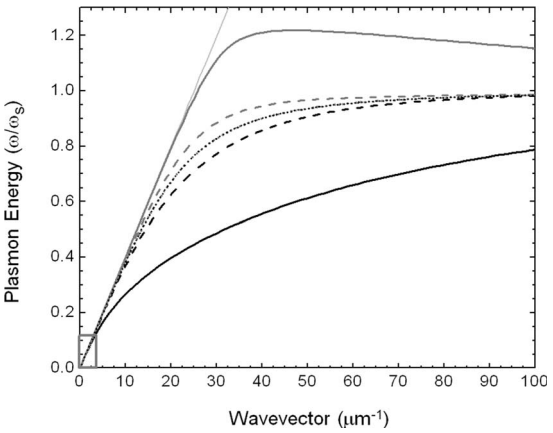

FIG. 1. Plasmon-dispersion relations calculated using Eq. (1) for films of thicknesses 0.01 (solid), 0.05 (dashed), and 10μm (dotted). The black curves are the short-range symmetric bonding film plasmon mode and the gray curves are the long-range antisymmetric antibonding film plasmon mode. The plasmon energies are normalized to the surface-plasmon frequency, $\omega_S(\omega_S=\omega_B/\sqrt{2})$. The light gray straight line represents the dispersion relation of a light in a vacuum and the small box denotes the THz region.

the surface plasmons associated with the two surfaces interact and form hybridized bonding (black) and antibonding (gray) film plasmon modes with different charge alignments. In Eq. (1), the "−" (+) sign on the right-hand side leads the bonding (antibonding) film plasmon which has lower (higher) energy and symmetrically (antisymmetrically) aligned surface charge densities between the upper and lower surfaces of the film. The energy splitting between the bonding and antibonding film plasmon depends on the thickness of the film. For a thick film ($t=10\mu$m), the splitting is very small and cannot be discerned in Fig. 1. In this limit, the right-hand side of Eq. (1) approaches zero and the dispersion relation for both film modes can be analytically solved as $k=\frac{\omega}{c}[\frac{\varepsilon_1(\omega)\varepsilon_0}{\varepsilon_1(\omega)+\varepsilon_0}]^{1/2}$.

The physical mechanism for the excitation of the HPR is illustrated in Fig. 2. On a perfect metallic film (without a hole), the film plasmons do not induce dipole moments and can therefore not couple to light. However, in the presence of a hole, the film plasmons can generate localized dipole moments due to the induced charge distributions along the edges of the hole. For an incident wave polarized parallel to the film surface, assuming the surface plasmon is a plane wave, the optimal coupling between the light and the short-range bonding mode occurs when half of the plasmon wavelength equals the diameter of a hole D, that is $\lambda/2\sim D$, as illustrated in the middle row of Fig. 2. At this wavelength, there is no coupling between the incident light and any long-range antibonding film plasmon since its induced electric dipole along the film is zero. For perpendicular polarization, the nature of the interactions is quite different. The optimal coupling condition illustrated in the lower row of Fig. 2 shows that the long-range antibonding film plasmon can couple with an incident perpendicularly polarized field when the wavelength of the plasmon resonance equals the diameter of a hole, that is, $\lambda\sim D$. The diagram also clearly shows that for perpendicular polarization, there can be no coupling of

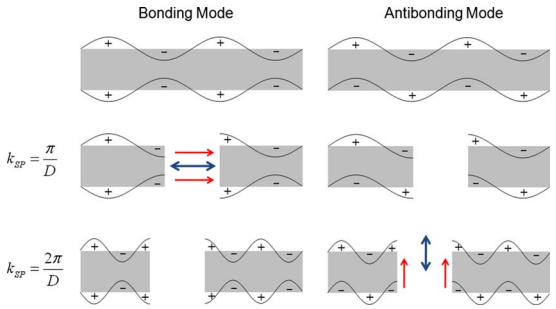

FIG. 2. (Color online) Upper row: electric-charge configuration for the bonding (left) and antibonding (right) film plasmon modes. Middle row: optimal coupling mechanism for parallel polarized light (blue arrow) and the induced dipole moment (red arrows) from a bonding film plasmon of half wavelength equal to the hole diameter. Lower row: optimal coupling mechanism for perpendicularly polarized light (blue arrow) and the induced dipole moment (red arrows) from an antibonding film plasmon of wavelength equal to the hole diameter.

the incident light to any short-range bonding film plasmon. The polarization-dependent and spectrally distinct characteristics of the two plasmon modes are important for distinguishing them experimentally.

In the visible or near-infrared wavelength range, individual holes with nanometer-scale diameters have shown a strong redshift of the HPR with increasing diameter or decreasing film thickness for light with parallel polarization.[16,17,24] The redshift can be explained in terms of coupling to the bonding film plasmon mode. For perpendicularly polarized light, the spectral position of the antibonding film plasmon mode would overlap other spectral features, such as interband transitions. Thus the observation of antibonding mode coupling has not previously been reported using visible or near IR light. Measurements in the THz frequency regime overcome this difficulty and moreover can provide a broad measurable dynamic range (in spectrum) which is capable of measuring several higher-order resonant modes at once. In this regime illustrated with the small box in Fig. 1, the dispersion of both the bonding and antibonding modes overlap and follow the light line. Even though the bonding and antibonding film plasmon energies are nearly degenerate in the THz regime, they are physically distinguishable since their coupling to electromagnetic radiation occurs at different frequencies and polarizations.

We used standard THz time-domain spectroscopy[25,26] to study the antibonding plasmon mode coupling of an individual hole in a thin metallic film. In order to generate a perpendicular component of the incident light, we tilt the sample with respect to the beam-propagation direction and perform angle-dependent transmission measurements. All the transmitted THz electric field amplitude spectra are normalized by those measured at zero incidence angle, which makes angle-dependent optical properties clear. In addition, for a single aperture on which the electromagnetic waves are obliquely incident, the ratio between the electromagnetic radiation impinging on the area of the single aperture and on the metal surfaces surrounding the aperture changes. As the incidence angle becomes larger, the effective area of the aper-

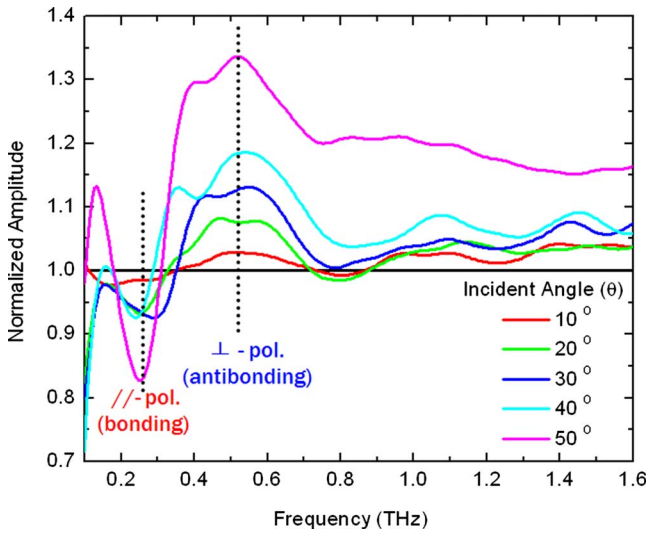

FIG. 3. (Color online) THz transmission amplitude spectra through a 700μm diameter hole fabricated by laser machining. A stainless-steel film used to make the hole has a thickness of about 10 μm which is much smaller than the wavelength of the incident THz radiation but much larger than the skin depth in the THz range. Angle-dependent THz transmission measurements are carried out by tilting the sample stage, varying the incidence angle θ of light from 0° to 50° with a step of 10°. These spectra are normalized to the one measured at normal incidence and also normalized by the effective area of the hole as seen by the incident THz beam, in order to highlight angle-dependent features. The dotted lines, located at the frequencies of 0.26 and 0.52 THz, represent the spectral positions of the bonding and antibonding film plasmon modes, respectively.

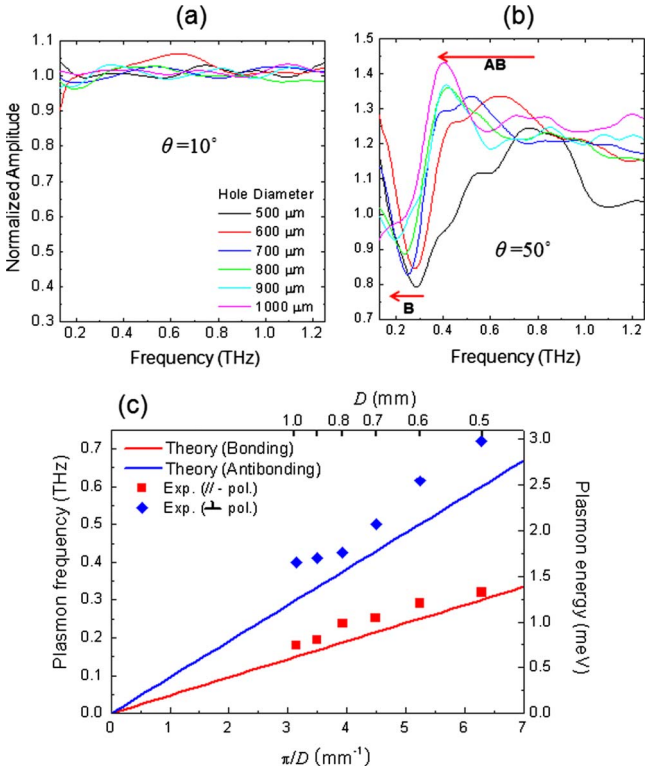

FIG. 4. (Color online) (a) Normalized THz transmission amplitude spectra, measured at the incidence angle of 10°, for different sizes of holes. There is no clear feature seen in the spectra. (b) Normalized THz transmission amplitude spectra measured at the incidence angle of 50°. The resonant peaks and dips due to the bonding and antibonding film plasmon coupling both show a strong redshift with increasing hole diameter. (c) Comparison between theoretical predictions and experimental measurement. The red (blue) line denotes the theoretically predicted hole plasmon resonance frequencies associated with the bonding (antibonding) film plasmon modes as a function of hole diameter. Red square (blue diamond) data points are obtained by the dip (peak) positions observed in the THz spectra, for different hole sizes.

ture becomes smaller. Therefore, the transmitted spectra are also normalized by this ratio.

Figure 3 shows the normalized THz electric field amplitude transmission spectra of a hole whose diameter is $D=700$ μm. In these normalized spectra, the HPR for the bonding film plasmon modes probed by the parallel component polarization of the incident light are expected to appear as dips since the parallel component of the light becomes smaller with increasing angle. On the contrary, the HPR for the antibonding modes arising from the perpendicular component of the light are expected to appear as peaks since the perpendicular component becomes larger. As shown in Fig. 3, the bonding mode coupling, which corresponds to the condition $\lambda/2=D$, appears as dips near 0.26 THz, whereas the antibonding mode coupling appears as peaks near 0.52 THz. Increasing the incidence angle makes the peaks and dips more pronounced. In addition, the spectral positions of the observed features do not shift with angle since they are determined only by the geometrical parameters of the hole.

To elucidate the existence of the antibonding film plasmon mode coupling further, we investigated the tunability of the resonance as a function of hole diameter. Figures 4(a) and 4(b) show the normalized THz transmission amplitude spectra for several sizes of holes from 500 to 1000 μm in diameter, measured at incidence angles of 10° and 50°, respectively. As in Fig. 3, these spectra are normalized to the transmission at normal incidence. For the incidence angle of 10°, the spectra do not show any obvious resonance since neither the total amount of perpendicularly polarized light nor the variation in parallel polarized light are sufficiently large. On the contrary, the spectra measured at the incidence angle of 50° show both spectral features prominently. Moreover, these resonances exhibit redshifts with the hole diameter. As predicted by the film plasmon dispersion, the energies of both the bonding (B) and antibonding (AB) film plasmon coupling exhibit a redshift with increasing hole diameter [red arrows in Fig. 4(b)].

In Fig. 4(c), we compare our theoretical prediction and the experimental data obtained from THz spectra. The data points marked as red squares (peaks) and blue diamonds (dips) depict the energies of the resonances obtained from the measured THz spectra for different sizes of holes. The experimental data points are located at slightly higher frequencies than the theoretical predictions denoted by the solid lines of Fig. 4(c). This is due to the fact that our simple theoretical model assumes an optimal coupling condition

based only on the hole diameter, essentially assuming that the hole is a rectangular slit with uniform size along its length. This model thus neglects the excitation of shorter wavelength (higher energy) film plasmons satisfying the resonant dipole condition across the shorter gaps of the hole than the diagonal diameter. Nevertheless, there is excellent consistency between theory and experiment. This constitutes convincing evidence for the observation of the antibonding film plasmon mode and shows that a subwavelength hole in a metallic film can serve as an antenna for launching film plasmons of different symmetry.

In conclusion, we have investigated the microscopic origin of the HPR for individual holes in thin metal films and shown experimental evidence of the coupling of polarized light and film plasmons using THz time-domain spectroscopy. Our results show that the optical coupling between long-range antibonding film plasmon modes and perpendicularly polarized light can be realized at a wavelength equal to the diameter of the hole. In addition, we demonstrate that selective excitation of short- and long-range film plasmon modes can be achieved by controlling the polarization. The results may be useful in future developments in optical plasmonic systems.

This research has been supported in part by the Korea Research Foundation under Grant No. KRF-2007–357-C00035, the National Science Foundation, and the Robert A. Welch Foundation.

*daniel@rice.edu

[1] T. W. Ebbesen, H. J. Lezec, H. F. Ghaemi, T. Thio, and P. A. Wolff, Nature (London) **391**, 667 (1998).
[2] W. L. Barnes, A. Dereux, and T. W. Ebbesen, Nature (London) **424**, 824 (2003).
[3] H. R. Stuart and D. G. Hall, Phys. Rev. Lett. **80**, 5663 (1998).
[4] P. Mühlschlegel, H. J. Eisler, O. J. F. Martin, B. Hecht, and D. W. Pohl, Science **308**, 1607 (2005).
[5] Y. Alaverdyan, B. Sepúlveda, L. Eurenius, E. Olsson, and M. Käll, Nat. Phys. **3**, 884 (2007).
[6] L. Novotny, Phys. Rev. Lett. **98**, 266802 (2007).
[7] A. H. J. Yang, Sean D. Moore, Bradley S. Schmidt, Matthew Klug, Michal Lipson, and David Erickson, Nature (London) **457**, 71 (2009).
[8] J. Le Perchec, P. Quémerais, A. Barbara, and T. Lópex-Ríos, Phys. Rev. Lett. **100**, 066408 (2008).
[9] A. V. Zayats, I. I. Smolyaninov, and A. A. Maradudin, Phys. Rep. **408**, 131 (2005).
[10] C. Genet and T. W. Ebbesen, Nature (London) **445**, 39 (2007).
[11] A. Degiron, H. J. Lezec, N. Yamamoto, and T. W. Ebbesen, Opt. Commun. **239**, 61 (2004).
[12] F. J. Garćia de Abajo, Opt. Express **10**, 1475 (2002).
[13] F. J. García Vidal, Esteban Moreno, J. A. Porto, and L. Martín Moreno, Phys. Rev. Lett. **95**, 103901 (2005).
[14] S. H. Chang, S. K. Gray, and G. C. Schatz, Opt. Express **13**, 3150 (2005).
[15] A. Y. Nikitin, D. Zueco, F. J. García Vidal, and L. Martín Moreno, Phys. Rev. B **78**, 165429 (2008).
[16] T. H. Park, Nikolay Mirin, J. Britt Lassiter, Colleen L. Nehl, Naomi J. Halas, and Peter Nordlander, ACS Nano **2**, 25 (2008).
[17] T. Rindzevicius, Yury Alaverdyan, Borja Sepulveda, Tavakol Pakizeh, and Mikael Käll, J. Phys. Chem. C **111**, 1207 (2007).
[18] T. H. Park and P. Nordlander, Chem. Phys. Lett. **472**, 228 (2009).
[19] Z. Yuan and S. Gao, Phys. Rev. B **73**, 155411 (2006).
[20] D. Sarid, Phys. Rev. Lett. **47**, 1927 (1981).
[21] V. N. Konopsky and E. V. Alieva, Phys. Rev. Lett. **97**, 253904 (2006).
[22] T. Okamoto, J. Simonen, and S. Kawata, Phys. Rev. B **77**, 115425 (2008).
[23] B. Hecht, H. Bielefeldt, L. Novotny, Y. Inouye, and D. W. Pohl, Phys. Rev. Lett. **77**, 1889 (1996).
[24] J. Prikulis, P. Hanarp, L. Olofsson, D. S. Sutherland, and M. Käll, Nano Lett. **4**, 1003 (2004).
[25] M. van Exter and D. Grischkowsky, Appl. Phys. Lett. **56**, 1694 (1990).
[26] Q. Wu, M. Litz, and X. C. Zhang, Appl. Phys. Lett. **68**, 2924 (1996).